JACS
JOURNAL OF THE AMERICAN CHEMICAL SOCIETY
pubs.acs.org/JACS
Article

Operando Infrared Spectroscopy Reveals the Dynamic Nature of Semiconductor–Electrolyte Interface in Multinary Metal Oxide Photoelectrodes

Anirudh Venugopal,* Recep Kas, Kayeu Hau, and Wilson A. Smith*

Cite This: J. Am. Chem. Soc. 2021, 143, 18581–18591
Read Online
ACCESS | Metrics & More | Article Recommendations | Supporting Information

ABSTRACT: Detailed knowledge about the semiconductor/electrolyte interface in photoelectrochemical (PEC) systems has been lacking because of the inherent difficulty of studying such interfaces, especially during operation. Current understandings of these interfaces are mostly from the extrapolation of ex situ data or from modeling approaches. Hence, there is a need for operando techniques to study such interfaces to develop a better understanding of PEC systems. Here, we use operando photoelectrochemical attenuated total reflection Fourier transform infrared (PEC-ATR-FTIR) spectroscopy to study the metal oxide/electrolyte interface, choosing $BiVO_4$ as a model photoanode. We demonstrate that preferential dissolution of vanadium occurs from the $BiVO_4$/water interface, upon illumination in open-circuit conditions, while both bismuth and vanadium dissolution occurs when an anodic potential is applied under illumination. This dynamic dissolution alters the surface Bi:V ratio over time, which subsequently alters the band bending in the space charge region. This further impacts the overall PEC performance of the photoelectrode, at a time scale very relevant for most lab-scale studies, and therefore has serious implications on the performance analysis and fundamental studies performed on this and other similar photoelectrodes.

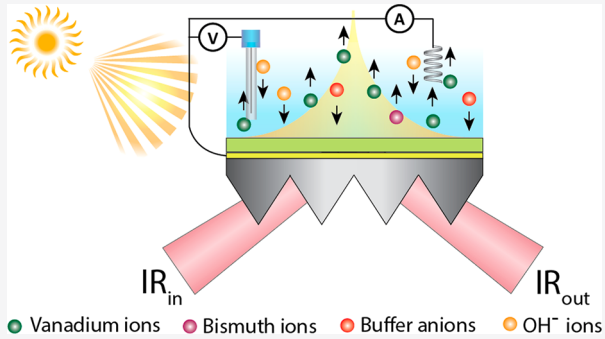

INTRODUCTION

Photoelectrochemical (PEC) water splitting is an attractive technological pathway to produce green hydrogen for low capacity, decentralized applications using only sunlight and water as the reactants.[1] Over the past few decades, metal oxide semiconductors have been extensively investigated for their use in photoelectrochemical systems for solar fuel synthesis and water treatment applications. Metal oxides are interesting candidates for such systems because of their perceived high stability and low cost and they satisfy the requirements of band positioning with respect to the water oxidation/reduction potentials.[1,2] They have been used either as a stand-alone photoelectrode[3,4] or as a passivation layer to protect smaller bandgap and less stable photoelectrodes,[5,6] and as a result the metal oxide/electrolyte interface is a vitally important aspect in photoelectrochemistry.

Most of the early research in photoelectrochemistry focused on finding metal oxides with a single metal component (referred to as binary metal oxides hereafter) that can satisfy the basic requirements of a photoelectrode. Soon it was apparent that these binary metal oxides are not sufficient due to their intrinsic limitations in light absorption, carrier transport, and/or stability.[7] To overcome some of these challenges, more recently, multinary metal oxides such as $BiVO_4$, $CuWO_4$, Fe_2TiO_5, and $CuBiO_4$ have been extensively investigated, as they offer us the ability to tune the optoelectronic properties of these photoelectrodes by varying the metal composition and defect structure in these multinary metal oxides.[1,7] Even though these materials have surpassed their binary counterparts in terms of performance and efficiency, they are still massively underperforming when compared to their theoretical efficiency limits. Charge carrier recombination at the semiconductor–electrolyte interface (SEI) has been cited as one of the main factors for this reduced performance.[8] Co-catalyst deposition has demonstrated the ability to partly alleviate this problem by improving the charge transfer kinetics of the holes toward water oxidation.[9,10] However, even with the addition of co-catalysts, these electrodes have not achieved their true potential. In addition, the use of co-catalysts will bring additional processing steps and costs in the manufacturing of these photoelectrodes and can also induce parasitic light absorption in these materials, making them a less attractive solution.[11]

Received: August 6, 2021
Published: November 2, 2021

ACS Publications
© 2021 The Authors. Published by American Chemical Society

https://doi.org/10.1021/jacs.1c08245
J. Am. Chem. Soc. 2021, 143, 18581–18591

To tackle this fundamental problem, there is a need to study and better understand the semiconductor−electrolyte interface. Such attempts have been limited because of the practical difficulty of studying such interfaces during photoelectrolysis. Most of the knowledge that we have at present about these interfaces has come indirectly from extrapolation of ex situ data or are based on modeling approaches. Only a handful of in situ[12−15] and operando studies[16] have been performed on these systems until now. Operando and in situ studies of these interfaces are of utmost importance, as only such works can reveal the true nature of the SEI. In this work, for the first time, we use operando ATR-FTIR spectroscopy to study the $BiVO_4$/electrolyte interface under PEC conditions. Previous works[16,17] done with PEC-ATR-FTIR spectroscopy on a hematite photoanode used an Otto configuration of ATR,[18] obtained by pressing the photoanode against the internal reflection element (IRE) with an ultrathin layer of electrolyte in between. Apart from the obvious compromise of the electrochemical aspects of such a configuration, the spectra were also dominated by the absorption of the bulk water, as the evanescent wave had to travel through the bulk water to get to the semiconductor/electrolyte interface. This meant that only a small window, not dominated by the water absorption, can be analyzed. Here, in a novel approach, ATR in a Kretschmann configuration[18] is used to study the metal oxide/electrolyte interface under operando conditions. A micromachined silicon wafer (∼500 μm) was used as the IRE to facilitate this. This thin wafer minimized the path length of infrared within the bulk of silicon and thus minimized the resultant phonon absorption of infrared by the bulk of silicon.[19] This way, the lower wavenumber limit (LWL) of this IRE was extended to ∼600 cm^{-1}, enabling the probing of the fingerprint region. Hence, an extended range of the infrared spectra of interest (600−4000 cm^{-1}) of the $BiVO_4$/electrolyte interface is revealed under electrochemical and photoelectrochemical conditions.

It is shown that, upon illumination in open-circuit conditions, the SEI is modified with time as a result of the dissolution of vanadium from the surface of $BiVO_4$ complexes. This dissolution modifies the space charge region and results in an improved charge separation and thus a better PEC performance because of the heterojunction formed by the vanadium-deficient surface $BiVO_4$ and the pristine bulk $BiVO_4$. This concept of improved PEC performance from prolonged illumination under open-circuit conditions is known as "photocharging" in previous literature.[20−23] The time scale of this effect was shown to be on the order of minutes to hours.[20−23] Until now, similar enhancements from photocharging have been demonstrated for $BiVO_4$,[20−23] $CuWO_4$,[24] Fe_2TiO_5,[25] and Bi_4TaO_8X[26] and in heavily doped binary metal oxide photoanodes,[27,28] indicating that this could be a common phenomenon in multinary metal oxide photoelectrodes. Hence, $BiVO_4$ is chosen in this work as a model multinary metal oxide photoelectrode, and as such, the findings here can be extended to other commonly used multinary metal oxide photoelectrodes. The time-scale of this dissolution and modification of the interface will have drastic implications on the performance analysis and in many fundamental studies that have been performed on these materials. Our ATR-FTIR spectroscopy data also reveal that most of the (photo)-electrochemical performance improvement techniques in the literature for improving the PEC performance of multinary metal oxide photoanodes[29,30] result in similar surface modification and heterojunction formation with the bulk electrode.

MATERIALS AND METHODS

Preparation of $BiVO_4$ Photoanodes. The bismuth vanadate thin film photoanodes were prepared using a spray pyrolysis technique. Details of the deposition procedure can be found here.[31] Briefly, clean FTO substrates (Hartford Glass Co.) were first spray coated with a ∼80 nm SnO_2 layer at 425 °C. Subsequently, a ∼200 nm $BiVO_4$ layer was coated on top at 450 °C. For the operando infrared spectroscopy, $BiVO_4$ was directly deposited on a clean silicon IRE (Specialized 1, Irubis GmbH), without the intermediate SnO_2 layer. A ∼20 nm conductive indium tin oxide (ITO) layer was sputtered onto this silicon IRE, before the deposition of $BiVO_4$. After the $BiVO_4$ deposition, the samples were annealed in air at 460 °C for 2 h, at a rate of 5 °C/min. The silicon IRE was cleaned by sonication in concentrated HCl, followed by multiple sonication steps in ultrapure water.

ITO Sputter Deposition. A ∼20 nm ITO layer was deposited by DC magnetron sputtering onto a micromachined Si ATR element (Specialized 1, Irubis GmbH) using an AJA Orion sputtering system. The thickness was chosen such that the layers are thick enough to have good electron conduction, but thin enough to minimize Drude absorption of the infrared by the conductive ITO layer. Prior to the deposition, the substrate was cleaned by sonication in concentrated hydrochloric acid followed by washing and sonication in ultrapure water. Further, the surface was cleaned using an argon plasma for 2 min at 20 W prior to the ITO deposition. The ITO layer was deposited at a rate of 0.169 Å/s from an ITO target (ITO 90−10%, 99.99% pure, Testbourne Ltd.) at 15 W, at a base pressure of 3 μbar, with substrate rotation.

Photoelectrochemical Testing. Photoelectrochemical measurements were performed using a custom-built photoelectrochemical cell, in a three-electrode configuration with a saturated Ag/AgCl reference electrode (XR300, Radiometer Analytical). A platinum coil was used as the counter electrode. Different electrolytes were used throughout this study and are mentioned specifically in the Results and Discussion sections. Potentials and currents during the experiments were measured and controlled using a VersaSTAT 3 potentiostat. The photoelectrochemical experiments were performed in a nitrogen gas purge at 50 sccm, to remove any dissolved gases, and with magnetic stirring to ensure adequate mixing. A Newport Sol3A Class AAA solar simulator was used in the experiments to provide a AM1.5G simulated solar illumination. Back-side illumination was used in all the experiments. The photocharging of the $BiVO_4$ photoanodes was performed by prolonged illumination of the photoanodes under open-circuit conditions.

Operando ATR-FTIR Spectroscopy. Operando ATR-FTIR measurements were performed in a Bruker Vertex 70 spectrometer equipped with a liquid nitrogen cooled MCT detector and a Veemax-III ATR accessory. The $BiVO_4$-coated Si IRE element was loaded onto a custom-built cell, which is then placed on the Veemax III ATR accessory, with a 35° angle of incidence. After loading, the setup was left idle for 30 min to purge out moisture and CO_2 before the start of experiments. Electrochemical connections were taken by making an electrical contact with the ITO back contact and a coiled platinum wire was used as the counter electrode. A PINE low-profile Ag/AgCl electrode was used as a reference, and the potentials were controlled using a BioLogic SP-200 potentiostat. Nitrogen gas was purged through the electrolyte at 50 sccm throughout the experiments. A ThorLabs MP405LP1 LED, equipped with a collimator, was used for illumination during the experiments, at a light intensity of 6 mW/cm^2. The light intensity was measured using a Newport 1919R hand-held power meter equipped with a 918D-UV-OD3R detector. The FTIR spectra were obtained in the absorbance mode, by averaging 512 scans. As such, each spectra presented here is an average of data measured over ∼80 s.

https://doi.org/10.1021/jacs.1c08245
J. Am. Chem. Soc. 2021, 143, 18581−18591

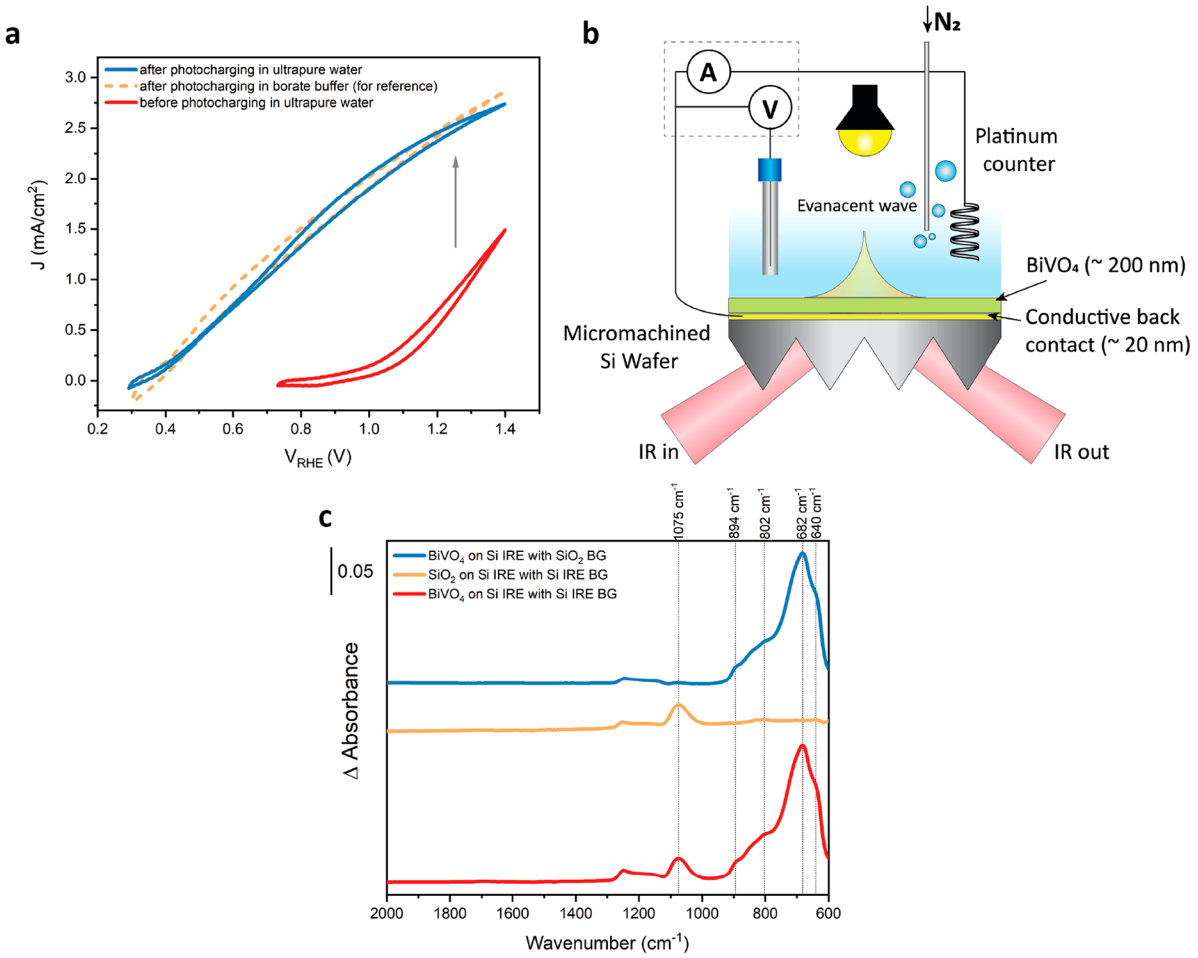

Figure 1. (a) Cyclic voltammogram of $BiVO_4$ before and after photocharging in ultrapure water, with the voltammetry performed in a borate buffer electrolyte. The voltammogram of $BiVO_4$ photocharged in a borate buffer is also shown for reference. (b) Schematic of the custom-built operando PEC-ATR-FTIR cell with a 405 nm LED light source, a saturated Ag/AgCl reference electrode, and a platinum counter. (c) Infrared spectra of the reference $BiVO_4$ thin film obtained with different backgrounds. Spectra of SiO_2 formed during the $BiVO_4$ deposition process is also shown.

RESULTS

In the present work, photocharging of $BiVO_4$ was performed in ultrapure water, unless otherwise specified, by prolonged illumination of the sample under open-circuit conditions. Figure 1(a) shows the cyclic voltammogram of $BiVO_4$ photoanodes before and after photocharging in ultrapure water. The voltammogram of $BiVO_4$ photocharged in a borate buffer is also shown in Figure 1(a) for reference. As evident here, the PEC performance of $BiVO_4$ improved multifold, post-photocharging, in accordance with previous literature.[20,21] This improvement was accompanied by a cathodic shift in the open-circuit potential (Figure S1(a)) and onset potential of the photocurrent. To study the $BiVO_4$/electrolyte interface under (photo)electrochemical condition, an operando PEC-ATR-FTIR spectroscopy setup was developed, and a schematic of this setup is shown in Figure 1(b). $BiVO_4$ was directly deposited onto the micromachined Si IRE element, after the deposition of a thin conductive ITO layer as a back contact. This configuration ensured that the evanescent wave first passes through the $BiVO_4$/electrolyte interface, before penetrating into the bulk of the electrolyte. In addition, a silicon wafer IRE facilitated annealing the $BiVO_4$ thin film, postdeposition at 460 °C, to ensure its transformation to a monoclinic scheelite structure.

The bulk infrared spectra of $BiVO_4$ are shown in Figure 1(c), and the spectrum of the ITO film can be found in Supporting Information Figure S2. A clean Si IRE was used as the background, and the spectra were obtained by background subtraction in the absorbance mode. Figure 1(c) also includes the spectra of a SiO_2 layer on the Si IRE, which were obtained against a Si background. A thick SiO_2 layer is formed on the Si IRE when subjected to high-temperature spray pyrolysis of $BiVO_4$, resulting in a broad feature between 1000 and 1300 cm^{-1}, centered around 1075 cm^{-1}. This region is ascribed to the Si−O−Si asymmetric stretching vibrations in SiO_2.[32,33] To obtain the SiO_2 spectra, the Si IRE was subjected to the high-temperature process for the same duration as spray pyrolysis, but without depositing $BiVO_4$ on top. The spectra of $BiVO_4$ after the background subtraction with a SiO_2-coated Si IRE are also shown in Figure 1(c). In monoclinic $BiVO_4$, each V atom is coordinated with four O atoms and each Bi atom is coordinated with eight O atoms. Each dodecahedral BiO_8 unit is surrounded by eight tetrahedral VO_4 units, and as such, each O atom is coordinated to two Bi and one V center.[34] As a result of the structural distortion in the monoclinic structure, the 4-fold symmetry is lost, resulting in two different V−O bond lengths and four different Bi−O bond lengths within a monoclinic scheelite structure.[34] Due to this low symmetry, many overlapping peaks appear in the infrared spectra,

https://doi.org/10.1021/jacs.1c08245
J. Am. Chem. Soc. 2021, 143, 18581−18591

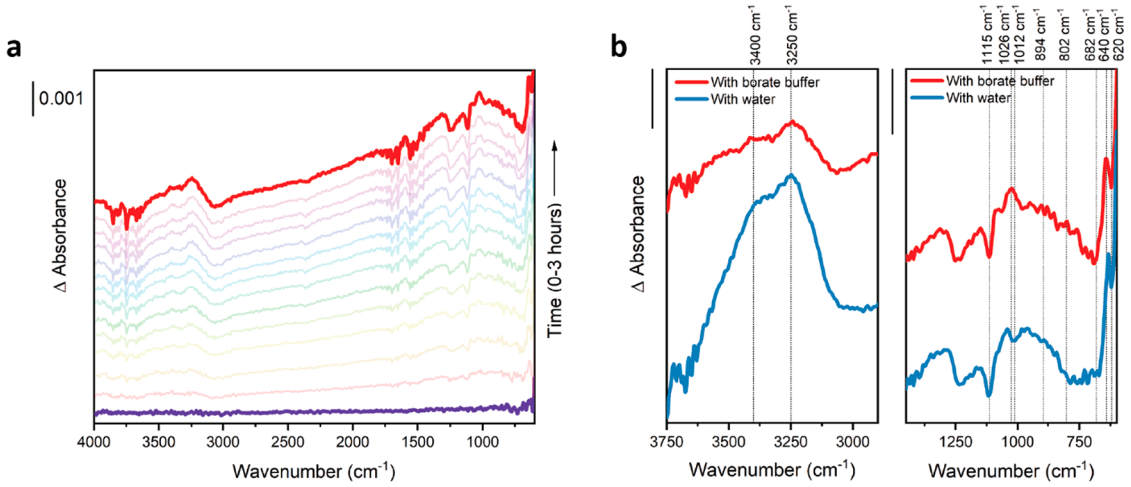

Figure 2. (a) Infrared spectra of the $BiVO_4$/electrolyte interface acquired over the course of photocharging in the case of a borate buffer electrolyte. (b) Comparison of relevant regions in the infrared spectra, after 3 h of photocharging in borate buffer electrolyte and in ultrapure water. The scale bar is 0.001 unit.

resulting in a very broad feature. As seen in Figure 1(c), the $BiVO_4$ FTIR spectrum is represented by a broad feature between 600 and 900 cm^{-1}, peaked around 682 cm^{-1} and with shoulder peaks on either side at 640, 802, 842, and 892 cm^{-1}. Although there is a general consensus in the literature that the infrared spectrum of monoclinic $BiVO_4$ has a broad feature in this region, the actual spectral shape and peak assignments vary across different works.[35−39] The discrepancies might stem from the differences in the synthesis technique used to prepare the monoclinic $BiVO_4$, a difference in post treatment procedures, and/or a difference in the characteristics of the sample used for the analysis (powder/thin film). All of these parameters can individually or collectively affect the vibrational frequencies of the resultant structure. For example, it was demonstrated that the symmetric and asymmetric stretching vibrations of the VO_4^{3-} units undergo a shift to lower wavenumbers with a higher annealing temperature.[39] In another instance, it was shown that monoclinic $BiVO_4$ with different dominant facets can have slightly different vibrational infrared spectra.[35] The broad peaks at 682 and 802 cm^{-1} in Figure 1(b) are tentatively assigned to the asymmetric stretching vibrations of the VO_4^{3-} unit, whereas the peak at 894 cm^{-1} is assigned to the symmetric stretching vibrations of this VO_4^{3-} unit. The shoulder peak at 640 cm^{-1} is assigned to the Bi−O symmetric stretching vibrations. Spectra of water were also acquired using this ATR-FTIR setup and are shown in Figure S2(b). The distinct spectra for borate ions and monobasic phosphate ions in water, acquired with water as the background, are also shown in Figure S2.

Next, the $BiVO_4$ was subjected to the photocharging treatment by illuminating the substrate in a borate buffer electrolyte (pH 10), under open-circuit conditions for 3 h in the custom-built operando PEC-ATR-FTIR cell. Cyclic voltammetry of this $BiVO_4$, before and after the photocharging treatment, is shown in Figure S3. The improvement in PEC performance here is very similar to that in the photoelectrochemical cell, indicating the successful reproduction of the photocharging effect in the operando cell. The change in the infrared spectra with time, acquired during the course of photocharging, in the case of borate buffer electrolyte is shown in Figure 2(a). The spectra were acquired after background subtraction, with an illuminated $BiVO_4$ sample under open-circuit conditions at t = 0 chosen as the background. This ensured that the changes in the infrared spectra due to any sub-minute electronic changes in $BiVO_4$ upon illumination were subtracted out from the resultant spectra and that the changes in the infrared spectra shown in Figure 2(a) are solely due to the photocharging process. Similarly, photocharging was also performed in ultrapure water and with a phosphate buffer. The changes in the infrared spectra and open-circuit potential in time are shown in Figure S4. In addition, the spectral changes of the ITO-coated Si IRE (i.e., without $BiVO_4$) in ultrapure water under illumination, $BiVO_4$ sample illuminated in air (i.e., without any electrolyte/water), and $BiVO_4$ sample left in the dark conditions in water were also obtained and are shown in Figure S5.

In Figure 2(a), many changes in the infrared spectra are visible over the course of photocharging. First, the spectra exhibit a positive tilt with time during photocharging. A rough baseline for the borate spectra after photocharging for 3 h is shown in Figure S4(d), showing the tilt of the spectra with photocharging. The positive tilt in the spectra is attributed to the Drude absorption of the infrared by the free electrons, which increases at lower wavenumbers. Therefore, an increase in the slope of the spectra with time suggests an increase in the free electron concentration in $BiVO_4$ with photocharging.[40] In fact, similar conclusions were also obtained from electrochemical impedance spectroscopy of photocharged $BiVO_4$.[20,22] In contrast, the $BiVO_4$ sample illuminated in air, i.e., with no electrolyte or water, and the non-illuminated $BiVO_4$ samples (Figure S5) do not attain a similar tilt, suggesting that the electrode/water interface and illumination are important here. This also coincides with the cathodic shift in the open-circuit potential with photocharging, as shown in Figure S4(b).

In Figure 2(b), the spectra of $BiVO_4$ after 3 h of photocharging in borate buffer electrolyte and ultrapure water are plotted together for comparison. Common spectral changes that were observed include a broad positive trending peak at 3250 and 3400 cm^{-1}, which is the region for OH stretching vibrations within the infrared spectra. A positive trending peak in this region suggests an increase in the concentration of OH/water species either at or close to the surface with increased photocharging. It should be noted that the increase in intensity of the OH stretching vibrations is only

https://doi.org/10.1021/jacs.1c08245
J. Am. Chem. Soc. 2021, 143, 18581−18591

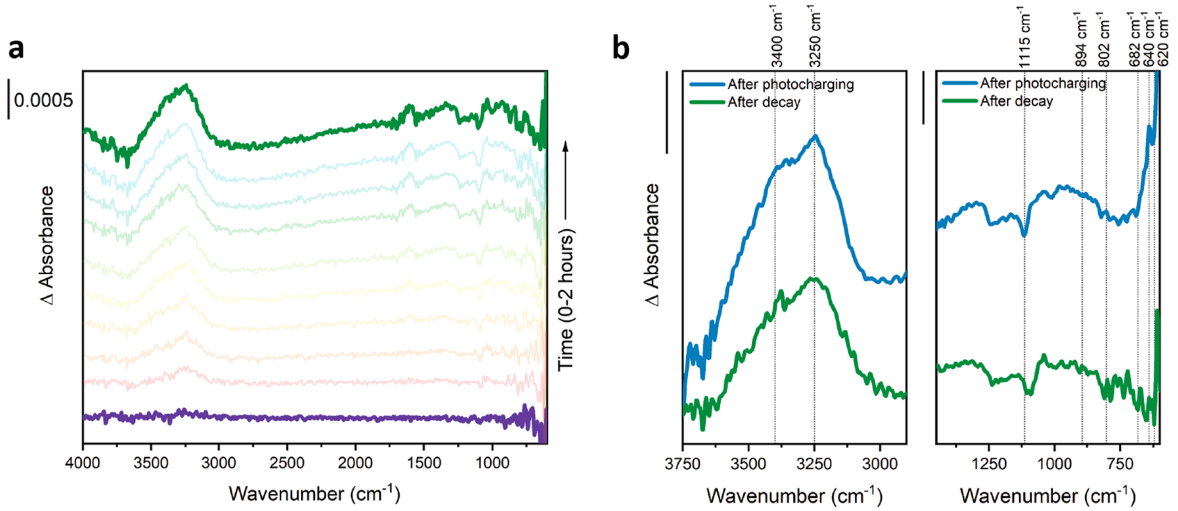

Figure 3. (a) Infrared spectra of the $BiVO_4$/electrolyte interface acquired over the course of the decay process in the dark in ultrapure water. (b) Comparison of the infrared spectra of $BiVO_4$ after 2 h of photocharging and decay in ultrapure water. The decay spectra were scaled by a factor of 2. The scale bar is 0.001 unit.

observed for illuminated samples. A $BiVO_4$ sample illuminated in air also showed a similar increase in intensity of the OH stretching vibrations with time, possibly as a result of the oxidation of moisture in the air by the photogenerated holes to form absorbed OH species at the $BiVO_4$ surface. The other common change is in the region of Si−O−Si and Si−Si/Si−H stretching vibrations. Here, a negative trending peak at 1115 cm^{-1} with a broad shoulder to its left is visible. Such negative trending peaks are seen in the case of SiO_2 when there is a breakage of the Si−O−Si bonds, resulting in $Si-O^-$ dangling bonds, which has a lower vibrational frequency.[33] A negative-going peak in this case implies that more Si−O−Si bonds are broken with increasing illumination time. The subsequently formed $Si-O^-$ bond is clearly visible with a positive trending peak at 1088 cm^{-1} in Figure S5(b). The origin of the negative-going peak at 620 cm^{-1} is more ambiguous. Peaks at 620 cm^{-1} have been reported for weak near-surface Si−Si stretching vibrations in amorphous silicon substrates. A negative-trending peak at 620 cm^{-1} is an indication of a change in the Si−Si stretching vibration with illumination, possibly suggesting the breakage of weak near-surface Si−Si bonds in the silicon-based IRE.[41] Alternatively, this negative-trending peak at 620 cm^{-1} could also be attributed to the wagging mode of Si−H bonds at the surface of the Si IRE. Si−H bonds could be formed at the surface during the acid cleaning step of the Si IRE and are now removed during the light treatment. These changes are also visible when the sample is illuminated in air, as seen in Figure S5(b). More research needs to be performed to reveal the exact identity of this peak at 620 cm^{-1}. Additionally, a small change in the background moisture and CO_2 content with time is also visible within the photocharging spectra due to the unusually long time scale of the measurements.

Both spectra in Figure 2(b) contain a negative-trending peak at 682 cm^{-1}, accompanied by a broad shoulder peak(s) to its left, which is also going down. The shape of this shoulder peak is slightly different in the case of borate and water. The peaks at 682 and 802 cm^{-1} were assigned to V−O asymmetric stretching vibrations, whereas the peak at 894 cm^{-1} was assigned to V−O symmetric stretching vibrations. It should also be noted that the intensity of the peak at 640 cm^{-1}, which was assigned to Bi−O symmetric stretching vibrations, is stable or only changes very slightly during photocharging. A decrease in the intensity of the V−O stretching vibration peaks with photocharging indicates a decrease in the concentration of vanadium from the $BiVO_4$ surface. It should be noted that this decrease in the intensity of the V−O stretching vibrations was not observed when $BiVO_4$ was illuminated in air. These data indicate that this decrease in the vanadium concentration is an interfacial process and that it only happens at the $BiVO_4$/water interface. The vanadium species is selectively removed from the surface during photocharging, leaving behind a bismuth-rich surface. X-ray photoelectron spectroscopy (XPS) data of photocharged $BiVO_4$, from previous reports,[20,23] also indicated a similar decrease in the surface vanadium concentration post-photocharging, which is in agreement with the observations from the infrared spectra of photocharged $BiVO_4$ in this work.

The other main difference in the spectra in Figure 2(b) of $BiVO_4$ photocharged in a borate buffer, compared to a sample photocharged in water, is in the region between 800 and 1050 cm^{-1}. In the case of borate, a positive-trending peak at 1026 cm^{-1} is visible. This peak is not visible in the case of water. Instead, a negative-trending peak at 1012 cm^{-1} is visible in the case of the sample photocharged in water, which is not seen in the case of borate buffer electrolyte. The peak at 1012 cm^{-1} is attributed to V═O stretching vibrations.[42−44] $BiVO_4$ can sometimes have V═O bonds at the surface due to the abrupt termination of the surface. The negative-trending peak at this position again suggests the removal of this vanadium species from the surface during photocharging. In the case of the borate buffer electrolyte, the positive-trending peak at 1026 cm^{-1} (and a broad peak underneath it) is assigned to an increase in the concentration of the borate/boric acid species in the inner sphere with photocharging.[45] A similar increase in the concentration of the electrolyte anionic species at the $BiVO_4$ surface with illumination was also observed with in situ hard X-ray XPS.[12] The broad positive-going peak of borate partially overlaps with the negative-going shoulder peak of the V−O stretching vibrations, explaining the difference in the shape of this shoulder peak between borate and water. The negative trending peak at 1012 cm^{-1} might also be present in the case of photocharging in borate buffer electrolyte, but it is

https://doi.org/10.1021/jacs.1c08245
J. Am. Chem. Soc. 2021, 143, 18581−18591

masked by the broad positive-going borate peaks and hence is not visible.

It has been shown in earlier reports that the photocharging effect was reversible in the dark.[21] This phenomenon occurred when the sample was left in open-circuit conditions in the dark for a prolonged time after photocharging, resulting in the enhancement effect from photocharging diminishing. This is observed by an inferior current−voltage response from cyclic voltammetry after the decay, when compared to a photocharged sample, as shown in Figure S6(a). The change in the infrared spectra during this dark decay process was also studied over time, and the spectra are shown in Figure 3(a). To make the identification easier, the spectrum after the 2 h dark decay process is compared with a sample photocharged for the same duration, and both spectra are shown in Figure 3(b). As seen with the photocharging process, the decay process also shows an increase in OH^-/water concentration near/at the surface with time. Additionally, the decreasing peak of Si−O−Si bond breakage at 1115 cm^{-1} that was present in the case of the photocharged sample is not visible in the case of the decayed sample. Instead, the dark sample has a decreasing peak at a slightly lower vibrational frequency, which was assigned to the stretching vibrations of Si−O^- species. Si−O^- species were formed from the bond breakage of the Si−O−Si under illumination, and the decreasing peak at this position for the decayed sample suggests the passivation or re-formation of these Si−O−Si bonds in the dark.

The main distinction between the infrared spectra of the photocharged sample and the decayed sample in Figure 3(b) is in the region between 600 and 900 cm^{-1}. As discussed before, during photocharging, the peaks ascribed to the V−O stretching vibrations decreased in intensity, while the peaks ascribed to the Bi−O stretching vibration at 640 cm^{-1} remained intact. In contrast, during the decay of the photocharging effect in the dark, a decreasing peak associated with the Bi−O stretching vibration was observed. On the other hand, the region of V−O stretching vibration is intact during this decay process. This suggests that the bismuth-rich surface formed during photocharging is slowly removed during the decay in the dark, further changing the Bi:V ratio at the $BiVO_4$ surface. The other main distinction is that the infrared spectra during the decay process do not tilt like the spectra in the case of photocharging. This is clear when the spectrum after 2 h of decay is compared to the spectrum after 2 h of photocharging in ultrapure water, as shown in Figure S6(b). Very small changes in the carrier concentration might occur in $BiVO_4$ even during the decay process because of the removal of bismuth ions in the dark (removal process could inject some electrons into the bulk). These small changes will have an effect on the slope of the spectra, but as shown in Figure S6(b), they are negligible when compared to the changes under illumination.

Further experiments were designed to mimic the photocharging of $BiVO_4$ in the dark by applying an anodic potential for a prolonged time. This was done to see if the PEC enhancement from photocharging can be replicated by providing an external applied voltage that is equivalent or higher than the photovoltage obtained from illumination. Although applying anodic potentials for prolonged times did not lead to enhancement in the PEC performance (Figure S7), further insights can be obtained on the dissolution of the photoanodes and its effect on the infrared spectrum. Therefore, the changes in the infrared spectra of the $BiVO_4$/electrolyte interface, when an anodic potential was applied under illuminated and dark conditions in a phosphate buffer electrolyte, were also studied in this work. In Figure 4(a), the

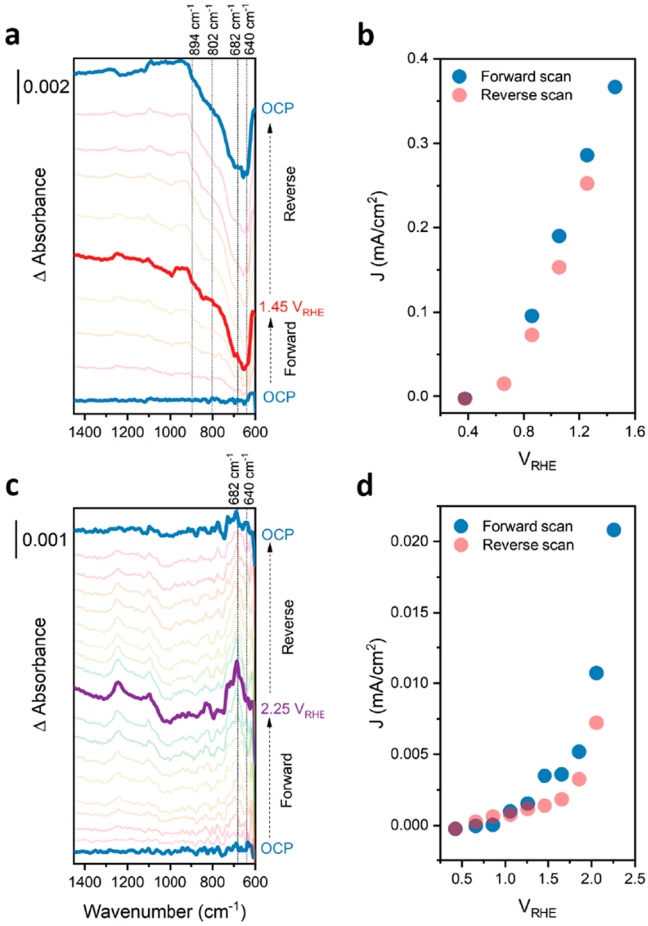

Figure 4. (a) Infrared spectra of the $BiVO_4$/electrolyte interface acquired at different anodic potentials during a potential step scan under illumination. (b) Current density versus applied potential plot when the potential was stepped under illumination. (c) Infrared spectra of the $BiVO_4$/electrolyte interface acquired at different potentials during a potential step scan in the dark. (d) Current density versus applied potential plot when the potential was stepped under dark conditions.

development of infrared spectra during a potential step scan of $BiVO_4$ under illumination is shown. Here, the potential was systematically changed (step size of 0.2 V) in ∼4 min intervals from open-circuit conditions to 1.45 V_{RHE} and then reversing the potential back to open circuit potential conditions in a similar stepwise manner, with the infrared spectra being recorded at each potential step. Initial open-circuit conditions were chosen as the background, for overall spectral background subtraction. The recorded current transient at the end of each potential step is plotted against the applied potential in Figure 4(b). Similarly, the infrared spectra were also recorded during a potential step scan in the dark conditions and are shown in Figure 4(c). Here the potential was stepped evenly from open-circuit conditions to 2.25 V_{RHE} and back to open-circuit conditions, and its current−voltage response is plotted in Figure 4(d). As discussed earlier, the region between 600 and 900 cm^{-1} in the infrared spectra is dominated by the absorption from the molecular vibrations in $BiVO_4$. It is

https://doi.org/10.1021/jacs.1c08245
J. Am. Chem. Soc. 2021, 143, 18581−18591

observed that the infrared spectra in Figure 4(a), when the potential is ramped up and cycled back to open-circuit conditions, are not completely reversible. Here, peaks at 640, 682, 802, and 894 cm^{-1}, pertaining to Bi−O and V−O stretching vibrations, are observed to increase in intensity in the negative direction with applied potential under illumination. It is interesting to note that both V−O and Bi−O stretching vibrations are going down in the case when a potential is applied in the presence of illumination, implying that both bismuth and vanadium are removed from the surface. In contrast, during photocharging, only the vanadium species were removed from the surface during the course of prolonged illumination. The larger intensity of the negative-going peaks suggests that the rate of this removal is also higher when a potential is applied in the presence of illumination. On the other hand, in the case of potential cycling in the dark in Figure 4(c), the region between 600 and 900 cm^{-1} seems to be completely reversible, implying that no bismuth or vanadium is removed from the surface during potential cycling in the dark. There are some potential-induced features that are visible within the infrared spectra in the dark between 600 and 900 cm^{-1}, but these features disappear when the potential is cycled back to open-circuit potential. These potential-induced features are attributed to potential-induced alterations of the molecular vibrations of $BiVO_4$ and/or to the vibrations from the surface-absorbed species, e.g., water oxidation intermediates, formed as a result of the applied anodic potential. Infrared signatures for different water oxidation intermediates on the $BiVO_4$ surface might also be expected when the potential is applied under illumination. The wavenumbers of these adsorbed intermediates are expected to be in the region of 700−950 cm^{-1}.[16] However, the strong overlap with the $BiVO_4$ bulk adsorption spectra and negative-trending peaks because of the cation dissolution, in this region, might overshadow the wavenumbers of these adsorbed intermediates, which typically have low intensities. The full-range spectra, in the case of applied potential under dark and illumination, are shown in Figure S8. The spectra in Figure 4(a) and (c) and Figure S8 also include some potential-induced changes in the OH stretching vibrations, and Si−O−Si stretching vibrations are also visible. The P−O stretching vibrations of the phosphate buffer ions have a strong overlap with the Si−O−Si stretching vibrations, and hence it is difficult to isolate and study any potential-induced changes of the buffer ions.

DISCUSSION

Prior research into the photocharging of $BiVO_4$ had indicated that the enhancement from photocharging is both a bulk and a surface effect.[20,21,23] In situ EXAFS and X-ray diffraction data suggested that the bulk structure of $BiVO_4$ was not effected with the photocharging treatment,[20,23] while intensity-modulated photocurrent spectroscopy (IMPS) on photocharged $BiVO_4$ suggested that the bulk charge separation and surface charge transfer improved upon photocharging.[22] All previous works on photocharging had been performed in the presence of a buffer electrolyte. Our recent work with grazing incidence X-ray Raman scattering had revealed that the space charge region was modified with the photocharging treatment, and it resulted in an increase in the band bending post-photocharging.[23] With the data available at that time, it was speculated that this was a result of the chemisorption of the buffer anions on the $BiVO_4$ surface and the resultant formation of a heterojunction close to the surface. In the current work, photocharging of $BiVO_4$ was performed in ultrapure water (i.e., no buffer anions present in the electrolyte), suggesting that the chemisorption of anions is not the primary reason for the photocharging process, contrary to our earlier speculations. These anions might still be playing a role in the photocharging process, which will be discussed later.

Operando infrared spectroscopy of the $BiVO_4$/water interface revealed that when an anodic potential is applied under illumination, both surface bismuth and vanadium ions are removed from the $BiVO_4$ surface. Similar observations were also made by Zhang et al.,[48] where they used operando inductively coupled plasma mass spectroscopy (ICPMS) to study the photostability of $BiVO_4$. The rates of dissolution of bismuth and vanadium were also observed to heavily depend on the nature of the co-ions in the electrolyte. Similarly, several works in the literature investigating the long-term PEC stability of $BiVO_4$ in similar conditions have observed a gradual increase in the photocurrent over the first few hours (∼20−30 h) of the stability tests, but have failed to unambiguously explain this behavior.[9,49] In the infrared spectroscopy data in this work, when $BiVO_4$ is illuminated under open-circuit conditions, only vanadium dissolution is observed from the $BiVO_4$ surface. When an anodic potential is applied in the dark conditions in a phosphate buffer electrolyte, the infrared spectra were completely reversible and no bismuth or vanadium dissolution was observed. This result also agrees with the work from Zhang et al.,[48] where they observed negligible dissolution of bismuth or vanadium when a potential was applied in the dark.

It should be noted from the above observations that the PEC performance enhancement with illumination (with or without applied potential) is always accompanied by the dissolution of bismuth and/or vanadium species. In contrast, when an anodic potential is applied in the dark conditions, no PEC performance enhancement or dissolution is observed. This indicates the dissolution of vanadium and/or bismuth is critical to have any observable PEC performance enhancement. The removal of vanadium and/or bismuth at different rates from the surface of $BiVO_4$, as in the case of photocharging or when an anodic potential is applied under illumination, will alter the Bi:V ratio at the surface over time. Typically, it is observed that the dissolution rates of bismuth are much lower than that of vanadium.[20,48] This change in the surface Bi:V ratio over time will also explain the change in the open-circuit potential over time that is seen during photocharging. Open-circuit potential, also known as corrosion potential, is a useful tool in corrosion chemistry to track the changes in the surface composition due to dissolution or formation of oxide/hydroxide.[50,51] Figure S9 shows the temporal evolution of the open-circuit potential and the change in the infrared absorbance at 682 cm^{-1} with time. As evident here, the change in the open-circuit potential with time closely follows the change in the infrared absorbance, confirming that they are directly related. The cathodic shift in the open-circuit potential during photocharging is thus also an indication of the change in the surface composition of $BiVO_4$.

The preferential removal of vanadium from the surface upon illumination will result in a bismuth-dominated surface on top of the pristine bulk $BiVO_4$. Gao et al. studied photopolarized $BiVO_4$ under a transmission electron microscope (TEM) and observed the development of a thin evenly distributed amorphous layer at the surface of $BiVO_4$, ∼3 nm thick, after prolonged photopolarization.[49] However, the exact composi-

https://doi.org/10.1021/jacs.1c08245
J. Am. Chem. Soc. 2021, 143, 18581−18591

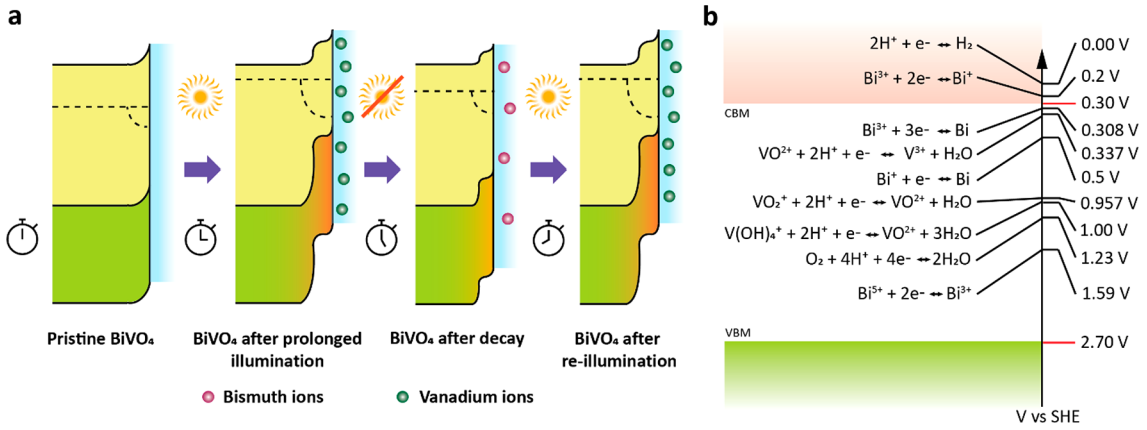

Figure 5. (a) Schematic of the dynamic nature of the metal oxide/electrolyte interface when subjected to illumination and dark cycle for a prolonged time, under open-circuit conditions. (b) Data of relevant standard reduction potentials plotted in the SHE scale along with the conduction band minimum (CBM) and valence band maximum (VBM) positions of $BiVO_4$. Data were aggregated from different sources.[46,47]

tion of this layer was not revealed. XPS data from previous works suggested an increase in the concentration of bismuth at the $BiVO_4$ surface post-photocharging.[20,23] The infrared data from the current work also indicate that surface vanadium is preferentially removed from the surface of $BiVO_4$ during photocharging. Therefore, it can be conclusively suggested that this amorphous layer is a result of the preferential vanadium dissolution upon illumination and thus leaves a bismuth-rich surface to form the SEI. A surface layer formation on the $BiVO_4$ surface by the chemisorption of anions from the electrolyte, in conditions akin to photocharging, was revealed using in situ hard X-ray XPS by Favaro et al.[12] The infrared spectra in this work also indicated an increase in the concentration of anionic OH^- and borate stretching vibrations with the removal of vanadium. These ions are possibly substituting the vacancies created by the removal of vanadium species, to maintain the charge balance. Therefore, the photocharging process can be considered as a sequential process where vanadium dissolution is followed by hydroxyl or anion uptake at the photoanode surface.

Lee et al.[52] recently reported the effect of surface composition on the PEC properties of $BiVO_4$. Their work suggested that a "bismuth-rich" bismuth vanadate will push the band edge positions toward the vacuum level. Such a shift in the band positions will result in a heterojunction between this bismuth-rich surface and the pristine bulk $BiVO_4$. This resultant heterojunction will increase the band bending within the space charge region and thereby improve the charge separation of photogenerated charge carriers close to the SEI. Improved PEC performance of a bismuth oxide coated bismuth vanadate photoelectrode was demonstrated by Ye et al.,[53] and the performance improvement was attributed to the electronic nature of the $Bi_2O_3/BiVO_4$ heterojunction. The improved charge separation within this heterojunction can also be responsible for the improved PEC performance observed after photocharging. Figure 5(a) summarizes this whole process from the formation of the heterojunction to the improved PEC performance. When pristine $BiVO_4$ is illuminated for a prolonged time, vanadium dissolution from the surface of $BiVO_4$ occurs, leaving behind a bismuth-rich surface. This bismuth-rich surface has band positions closer to the vacuum level and thus results in a heterojunction between the bismuth-rich surface and pristine bulk $BiVO_4$. It should be noted that the exact composition of this surface layer is not clear yet. This layer can be a complex mix of BiO_x, $BiVO_4$ with a bismuth-rich surface, and a bismuth borate layer (in the presence of a borate buffer). All these layers have the tendency to push the band positions at the surface closer to the vacuum level, thus creating a heterojunction and improving the band bending in the space charge region. When the photocharged $BiVO_4$ is further subjected to the decay process in the dark, slow bismuth dissolution occurs, reducing the band bending within this heterojunction. On re-exposure to prolonged illumination, the cycle repeats. In essence, any surface treatment technique that alters the surface Bi:V ratio of $BiVO_4$, or any multinary metal oxide, might produce a similar PEC performance enhancement. It has been previously reported in the literature that applying a cathodic potential in the dark to $BiVO_4$ for a short duration significantly improved its PEC performance.[29] It was suggested here that the enhancement is a result of the creation of "oxygen vacancies" as a result of the reduction process. We also looked into this process by applying a potential cathodic with respect to the open-circuit potential in the dark and recording the infrared spectra. As shown in Figure S10, the surface Bi:V ratio can also be altered by applying a cathodic potential in the dark for a short duration. This will also result in a similar heterojunction formation and provide similar enhancements as in the case of photocharging.

Information regarding the exact mechanism behind the corrosion of $BiVO_4$ is lacking in the literature. Different possibilities have been suggested for this, including oxidation of Bi^{3+} to Bi^{5+} and oxidation of lattice O^{2-} to O^- at the $BiVO_4$ surface by the photogenerated holes.[54] These oxidation processes can destabilize the lattice and induce corrosion of bismuth and/or vanadium. V^{5+} in $BiVO_4$ is already at its highest valency and thus cannot be oxidized further. However, V^{5+} at the surface can be reduced to V^{4+}/V^{3+} in the presence of water/protons by photogenerated electrons at the surface of $BiVO_4$. All these alternatives are thermodynamically possible, as summarized in Figure 5(b). The thermodynamic equilibrium data of the lattice oxygen oxidation process in $BiVO_4$ were not available. From the infrared spectroscopy data during photocharging, a decrease in the V−O stretching vibration was observed while the Bi−O stretching vibrations remained intact. This would suggest that the corrosion process is initiated either by the oxidation of lattice O or by reduction of V^{5+} at the surface of $BiVO_4$ and subsequent dissolution of vanadium. In

https://doi.org/10.1021/jacs.1c08245
J. Am. Chem. Soc. 2021, 143, 18581−18591

situ hard X-ray XPS data on $BiVO_4$ in similar photocharging conditions revealed that the oxidation state of bismuth remained unchanged at +3 upon illumination.[12] The O 1s XPS data from their work and other works[20,23] however showed a shoulder peak at ~531.5 eV, which was attributed to oxygen in surface-absorbed species, but could also be a result of the formation of O^- species at the surface.[55] When an anodic potential is applied under illumination, the intensity of both V−O and Bi−O stretching vibrations decreased. With the application of an anodic potential in addition to the illumination, there is potentially more driving force for the two-electron oxidation of Bi^{3+}, inducing bismuth dissolution along with vanadium, as observed in this work. The oxidation of surface bismuth and oxygen is very slow when an anodic potential is applied in the dark conditions, owing to the low carrier concentrations in the dark. This explains why no bismuth or vanadium dissolution was observed when the potential was cycled in the dark conditions.

CONCLUSIONS

An operando PEC-ATR-FTIR spectroscopy setup was developed and used to study the $BiVO_4$/electrolyte interface during water electrolysis. Operando measurements suggest that, upon illumination in open-circuit conditions, preferential dissolution of vanadium occurs from the $BiVO_4$ surface, which indirectly enhances the PEC performance of the photoanode. In contrast, when an anodic potential is applied under illuminated conditions, dissolution of both bismuth and vanadium was observed. Remarkably, it was noted that cation dissolution from $BiVO_4$ is almost always accompanied by improved PEC performance. Our experiments indicate that the difference in the dissolution rates of vanadium and/or bismuth under illumination alters the surface Bi:V ratio and results in a bismuth-rich surface on top of the pristine bulk $BiVO_4$. This is considered to create a heterojunction between the bismuth-rich surface and the pristine bulk $BiVO_4$, which significantly improves band bending near the interface. We believe that the improvement in band bending is directly responsible for improved PEC performance from the photocharging treatment. The slow dissolution rates of the cations from $BiVO_4$ imply that the semiconductor/electrolyte interface is slowly modified over time, and hence this interface is very dynamic. Our results also suggest that the change in the open-circuit potential over time, rather than the photocurrent, is a better indicator of the stability of the photoanode material or of the semiconductor/electrolyte interface.

$BiVO_4$ was used as a model multinary photoanode in this study; however, similar PEC performance enhancements from photocharging have been reported for other multinary metal oxides such as $CuWO_4$ and Fe_2TiO_5 and in heavily doped metal oxide photoelectrodes,[24−27] suggesting that this might be a very common phenomenon in different multinary metal oxide photoelectrodes. The time scale of this dissolution (minutes to hours) implies that this effect is very relevant to a lot of lab-scale studies and fundamental research performed on these materials and, as such, should be accounted for.

ASSOCIATED CONTENT

Supporting Information

The Supporting Information is available free of charge at https://pubs.acs.org/doi/10.1021/jacs.1c08245.

Additional experimental data including (photo-)electrochemical characterization of the electrodes, infrared spectroscopy measurements, and additional discussion (PDF)

AUTHOR INFORMATION

Corresponding Authors

Anirudh Venugopal − *Materials for Energy Conversion and Storage (MECS), Department of Chemical Engineering, Faculty of Applied Sciences, Delft University of Technology, Delft 2629HZ, The Netherlands;* orcid.org/0000-0003-3046-4749; Email: a.venugopal@tudelft.nl

Wilson A. Smith − *Materials for Energy Conversion and Storage (MECS), Department of Chemical Engineering, Faculty of Applied Sciences, Delft University of Technology, Delft 2629HZ, The Netherlands; Renewable and Sustainable Energy Institute (RASEI), University of Colorado Boulder, Boulder, Colorado 80303, United States;* orcid.org/0000-0001-7757-5281; Email: wilson.smith@nrel.gov

Authors

Recep Kas − *Renewable and Sustainable Energy Institute (RASEI), University of Colorado Boulder, Boulder, Colorado 80303, United States;* orcid.org/0000-0003-0508-5894

Kayeu Hau − *Materials for Energy Conversion and Storage (MECS), Department of Chemical Engineering, Faculty of Applied Sciences, Delft University of Technology, Delft 2629HZ, The Netherlands;* orcid.org/0000-0002-1991-9776

Complete contact information is available at: https://pubs.acs.org/10.1021/jacs.1c08245

Notes

The authors declare no competing financial interest.

ACKNOWLEDGMENTS

We thank Ir. Herman Schreuders and Ir. Joost Middlekoop for their help in building the operando PEC-ATR-FTIR setup. This work was financed by The Netherlands Organisation for Scientific Research (NWO) Vidi grant awarded to W.A.S.

REFERENCES

(1) van de Krol, R.; Grätzel, M. *Photoelectrochemical Hydrogen Production*; Springer: New York, 2012.

(2) Yang, Y.; et al. Progress in Developing Metal Oxide Nanomaterials for Photoelectrochemical Water Splitting. *Adv. Energy Mater.* **2017**, *7*, 1−26.

(3) Huang, D.; et al. 3.17% efficient Cu_2ZnSnS_4 - $BiVO_4$ integrated tandem cell for standalone overall solar water splitting. *Energy Environ. Sci.* **2021**, *14*, 1480−1489.

(4) Pan, L.; et al. Boosting the performance of Cu_2O photocathodes for unassisted solar water splitting devices. *Nat. Catal.* **2018**, *1*, 412−420.

(5) Digdaya, I. A.; et al. Extracting large photovoltages from a-SiC photocathodes with an amorphous TiO_2 front surface field layer for solar hydrogen evolution. *Energy Environ. Sci.* **2015**, *8*, 1585−1593.

(6) Bae, D.; Seger, B.; Vesborg, P. C. K.; Hansen, O.; Chorkendorff, I. Strategies for stable water splitting: via protected photoelectrodes. *Chem. Soc. Rev.* **2017**, *46*, 1933−1954.

(7) Gim, S.; Bisquert, J. *Photoelectrochemical Solar Fuel Production*; Springer: Cham, 2016.

(8) Zachäus, C.; Abdi, F. F.; Peter, L. M.; Van De Krol, R. Photocurrent of $BiVO_4$ is limited by surface recombination, not surface catalysis. *Chem. Sci.* **2017**, *8*, 3712−3719.

(9) Lee, D. K.; Choi, K. S. Enhancing long-term photostability of $BiVO_4$ photoanodes for solar water splitting by tuning electrolyte composition. *Nat. Energy* **2018**, *3*, 53−60.
(10) Zhong, D. K.; Choi, S.; Gamelin, D. R. Near-complete suppression of surface recombination in solar photoelectrolysis by 'co-Pi' catalyst-modified W:$BiVO_4$. *J. Am. Chem. Soc.* **2011**, *133*, 18370−18377.
(11) Trotochaud, L.; Mills, T. J.; Boettcher, S. W. An optocatalytic model for semiconductor−catalyst water-splitting photoelectrodes based on in situ optical measurements on operational catalysts. *J. Phys. Chem. Lett.* **2013**, *4*, 931−935.
(12) Favaro, M.; et al. Light-Induced Surface Reactions at the Bismuth Vanadate/Potassium Phosphate Interface. *J. Phys. Chem. B* **2018**, *122*, 801−809.
(13) Nakamura, R.; Nakato, Y. Primary Intermediates of Oxygen Photoevolution Reaction on TiO_2 (Rutile) Particles, Revealed by in Situ FTIR Absorption and Photoluminescence Measurements. *J. Am. Chem. Soc.* **2004**, *126*, 1290−1298.
(14) Nakamura, R.; Imanishi, A.; Murakoshi, K.; Nakato, Y. In situ FTIR studies of pimary intermediates of photocatalytic reactions on nanocrystalline TiO_2 films in contact with aqueous solutions. *J. Am. Chem. Soc.* **2003**, *125*, 7443−7450.
(15) Imanishi, A.; Okamura, T.; Ohashi, N.; Nakamura, R.; Nakato, Y. Mechanism of water photooxidation reaction at atomically flat TiO_2 (rutile) (110) and (100) surfaces: Dependence on solution pH. *J. Am. Chem. Soc.* **2007**, *129*, 11569−11578.
(16) Zandi, O.; Hamann, T. W. Determination of photo-electrochemical water oxidation intermediates on haematite electrode surfaces using operando infrared spectroscopy. *Nat. Chem.* **2016**, *8*, 778−783.
(17) Zhang, Y.; et al. Rate-Limiting O-O Bond Formation Pathways for Water Oxidation on Hematite Photoanode. *J. Am. Chem. Soc.* **2018**, *140*, 3264−3269.
(18) Kas, R.; et al. In-Situ Infrared Spectroscopy Applied to the Study of the Electrocatalytic Reduction of CO_2: Theory, Practice and Challenges. *ChemPhysChem* **2019**, *20*, 2904−2925.
(19) Morhart, T. A.; Unni, B.; Lardner, M. J.; Burgess, I. J. Electrochemical ATR-SEIRAS Using Low-Cost, Micromachined Si Wafers. *Anal. Chem.* **2017**, *89*, 11818−11824.
(20) Trześniewski, B. J.; et al. Near-complete suppression of surface losses and total internal quantum efficiency in $BiVO_4$ photoanodes. *Energy Environ. Sci.* **2017**, *10*, 1517−1529.
(21) Trześniewski, B. J.; Smith, W. A. Photocharged $BiVO_4$ photoanodes for improved solar water splitting. *J. Mater. Chem. A* **2016**, *4*, 2919−2926.
(22) Liu, E. Y.; Thorne, J. E.; He, Y.; Wang, D. Understanding Photocharging Effects on Bismuth Vanadate. *ACS Appl. Mater. Interfaces* **2017**, *9*, 22083−22087.
(23) Firet, N. J.; et al. Chemisorption of Anionic Species from the Electrolyte Alters the Surface Electronic Structure and Composition of Photocharged $BiVO_4$. *Chem. Mater.* **2019**, *31*, 7453−7462.
(24) Venugopal, A.; Smith, W. A. Light induced formation of a surface heterojunction in photocharged $CuWO_4$ photoanodes. *Faraday Discuss.* **2019**, *215*, 175−191.
(25) Deng, J.; Lv, X.; Zhong, J. Photocharged Fe_2TiO_5 /Fe_2O_3 Photoanode for Enhanced Photoelectrochemical Water Oxidation. *J. Phys. Chem. C* **2018**, *122*, 29268−29273.
(26) Tao, X.; et al. Photoinduced Surface Activation of Semi-conductor Photocatalysts under Reaction Conditions: A Commonly Overlooked Phenomenon in Photocatalysis. *ACS Catal.* **2020**, *10*, 5941−5948.
(27) Xie, J.; Yang, P.; Liang, X.; Xiong, J. Self-Improvement of Ti:Fe_2O_3 Photoanodes: Photoelectrocatalysis Improvement after Long-Term Stability Testing in Alkaline Electrolyte. *ACS Appl. Energy Mater.* **2018**, *1*, 2769−2775.
(28) Tayebi, M.; Tayyebi, A.; Lee, B. K. Photocharged molybdenum-doped $BiVO_4$ photoanodes for simultaneous enhance-ments in charge transport and surface passivation. *Sol. Energy* **2019**, *191*, 427−434.
(29) Wang, S.; Chen, P.; Yun, J.-H.; Hu, Y.; Wang, L. An Electrochemically Treated $BiVO_4$ Photoanode for Efficient Photo-electrochemical Water Splitting. *Angew. Chem.* **2017**, *129*, 8620−8624.
(30) Meng, Q.; et al. Efficient $BiVO_4$ Photoanodes by Postsynthetic Treatment: Remarkable Improvements in Photoelectrochemical Performance from Facile Borate Modification. *Angew. Chem., Int. Ed.* **2019**, *58*, 19027−19033.
(31) Abdi, F. F.; Firet, N.; van de Krol, R. Efficient $BiVO_4$ Thin Film Photoanodes Modified with Cobalt Phosphate Catalyst and W-doping. *ChemCatChem* **2013**, *5*, 490−496.
(32) Rappich, J.; Lewerenz, H. J. Photo- and potential-controlled nanoporous silicon formation on n-Si(111): An in-situ FTIR investigation. *Thin Solid Films* **1996**, *276*, 25−28.
(33) Amekura, H.; Umeda, N.; Okubo, N.; Kishimoto, N. Ion-induced frequency shift of ∼1100 cm^{-1} IR vibration in implanted SiO_2: Compaction versus bond-breaking. *Nucl. Instrum. Methods Phys. Res., Sect. B* **2003**, *206*, 1101−1105.
(34) Fatwa Firdaus, A. Towards highly efficient bias-free solar water splitting. PhD Thesis, TU Delft, 2013.
(35) Baral, B.; Parida, K. {040/110} Facet Isotype Heterojunctions with Monoclinic Scheelite BiVO4. *Inorg. Chem.* **2020**, *59*, 10328−10342.
(36) Frost, R. L.; Henry, D. A.; Weier, M. L.; Martens, W. Raman spectroscopy of three polymorphs of $BiVO_4$: Clinobisvanite, dreyerite and pucherite, with comparisons to $(VO_4)_3$- bearing minerals: namibite, pottsite and schumacherite. *J. Raman Spectrosc.* **2006**, *37*, 722−732.
(37) Gotić, M.; Musić, S.; Ivanda, M.; Šoufek, M.; Popović, S. Synthesis and characterisation of bismuth(III) vanadate. *J. Mol. Struct.* **2005**, *744−747*, 535−540.
(38) Longchin, P.; et al. Characterization of bismuth vanadate ($BiVO_4$) nanoparticle prepared by solvothermal method. *Integr. Ferroelectr.* **2016**, *175*, 18−24.
(39) Pookmanee, P.; Kojinok, S.; Puntharod, R.; Sangsrichan, S.; Phanichphant, S. Preparation and characterization of $BiVO_4$ powder by the sol-gel method. *Ferroelectrics* **2013**, *456*, 45−54.
(40) Karabudak, E.; et al. On the pathway of photoexcited electrons: Probing photon-to-electron and photon-to-phonon conversions in silicon by ATR-IR. *Phys. Chem. Chem. Phys.* **2012**, *14*, 10882−10885.
(41) Oh, Y.-J.; Cho, S. M.; Chung, C.-H. An In Situ ATR-FTIR Study on Palladium Displacement Reaction on Hydrogen-Terminated Silicon Surface. *J. Electrochem. Soc.* **2005**, *152*, C348.
(42) O'Dwyer, C.; et al. Vanadate Conformation Variations in Vanadium Pentoxide Nanostructures. *J. Electrochem. Soc.* **2007**, *154*, K29.
(43) Marzouk, M. A.; El-Kheshen, A. A.; Sayed Ahmed, S. A.; Aboelenin, R. M. M. Spectroscopic Studies on Nano-Single Crystal $BiVO_4$ Glass Ceramic as Dye Degradation for Wastewater Purification. *Silicon* **2018**, *10*, 509−517.
(44) Ramana, C. V.; Hussain, O. M.; Pinto, R.; Julien, C. M. Microstructural features of pulsed-laser deposited V_2O_5 thin films. *Appl. Surf. Sci.* **2003**, *207*, 135−138.
(45) Peak, D.; Luther, G. W.; Sparks, D. L. ATR-FTIR spectroscopic studies of boric acid adsorption on hydrous ferric oxide. *Geochim. Cosmochim. Acta* **2003**, *67*, 2551−2560.
(46) Hermans, Y.; et al. Analysis of the interfacial characteristics of BiVO4/metal oxide heterostructures and its implication on their junction properties. *Phys. Chem. Chem. Phys.* **2019**, *21*, 5086−5096.
(47) Vanysek, P. Electrochemical Series. *CRC Handb. Chem. Phys.* **2000**, *8* (8), 665−671.
(48) Zhang, S.; et al. Different photostability of BiVO4in near-pH-neutral electrolytes. *ACS Appl. Energy Mater.* **2020**, *3*, 9523−9527.
(49) Gao, R.; Wang, L. Stable Cocatalyst-Free BiVO 4 Photoanodes with Passivated Surface States for Photocorrosion Inhibition. *Angew. Chem.* **2020**, *132*, 23294−23299.
(50) Zhang, X. G. Corrosion Potential and Corrosion Current. In *Corrosion and Electrochemistry of Zinc*; Springer Science & Business Media, 1996; pp 125−156.

https://doi.org/10.1021/jacs.1c08245
J. Am. Chem. Soc. 2021, 143, 18581−18591

(51) Momeni, M.; Wren, J. C. A mechanistic model for oxide growth and dissolution during corrosion of Cr-containing alloys. *Faraday Discuss.* **2015**, *180*, 113−135.
(52) Lee, D.; et al. The impact of surface composition on the interfacial energetics and photoelectrochemical properties of BiVO4. *Nat. Energy* **2021**, *6*, 287−294.
(53) Ye, K. H.; et al. Facile synthesis of bismuth oxide/bismuth vanadate heterostructures for efficient photoelectrochemical cells. *RSC Adv.* **2015**, *5*, 34152−34156.
(54) Toma, F. M.et al. Mechanistic insights into chemical and photochemical transformations of bismuth vanadate photoanodes. *Nat. Commun.* **2016**, *7*, 1−11.
(55) Dupin, J. C.; Gonbeau, D.; Vinatier, P.; Levasseur, A. Systematic XPS studies of metal oxides, hydroxides and peroxides. *Phys. Chem. Chem. Phys.* **2000**, *2*, 1319−1324.

https://doi.org/10.1021/jacs.1c08245
J. Am. Chem. Soc. 2021, 143, 18581−18591